INTERNATIONAL JOURNAL OF CIRCUIT THEORY AND APPLICATIONS
Int. J. Circ. Theor. Appl. (2010)
Published online in Wiley InterScience (www.interscience.wiley.com). DOI: XX.XXXX/cta.XXX

Dynamics of PFC power converters subject to time-delayed feedback control

Abdelali El Aroudi[1,*,†] and Mohamed Orabi[2]

[1] *Departament d'Enginyeria ElectrÃ²nica, ElÃctricaiAutomÃ tica(DEEEA)*
Universitat Rovira i Virgili, Tarragona, Spain,
[2] *APEARC, South Valley University Aswan, Egypt*

SUMMARY

Power factor correction converters are power electronics circuits used as AC-DC power supplies. These systems are well known to exhibit nonlinear phenomena such as subharmonic oscillations and chaotic regimes. These undesirable behaviors increase the total harmonic distortion and therefore can jeopardize enormously the system performances. In this paper, time delay feedback control is applied to stabilize a two-stage power factor correction AC-DC converter when it exhibits these instabilities under traditional controllers. This control technique introduces many advantages to the most and widely used average current mode control through widening the stability domain of the system. By appropriately selecting the time delay feedback gain and the time delay period, the undesirable subharmonic components are eliminated while the desired ones remain unchanged. A harmonic balance approach is used for studying the dynamics of the system under the new control scheme and to obtain the stabilization domain. Copyright © 2010 John Wiley & Sons, Ltd.

KEY WORDS: Boost, PFC, AC-DC, Time Delay Feedback Control (TDFC), Harmonic Balance (HB), Instability, Subharmonics, Chaos.

1. Introduction

Power Factor Correction (PFC) circuits are suitable practical power supplies for regulating an output voltage while providing a near unity Power Factor (PF) [1]-[5]. With the increasing demand for power from the AC line and more constraints for power quality, PFC has attracted the interests of many researchers during the last years and many works have dealt with this area of research. Some of these works focused on PFC topologies for specific applications like [6], [7] while others were about the controller design of these systems and its improvement [8]-[10]. Although, a variety of circuit topologies and control methods have been developed for the PFC application, the boost and flyback converters working in Discontinuous Conduction Mode (DCM) are well suited for low power applications, while Continuous Conduction Mode

*Correspondence to: Abdelali El Aroudi, Departament d'Enginyeria Electrónica, Eléctrica i Automática (DEEEA)
Universitat Rovira i Virgili, Tarragona, Spain.
†E-mail: abdelali.elaroudi@urv.cat

Received 09-Aug-2009
Revised 08-Dec-2009
Accepted 07-Mar-2010

(CCM) boost converter with Average Current Mode (ACM) control, is commonly chosen for many medium and high power applications because of low conduction losses, reduced EMI filtering requirements, high DC gain (zero static error for the input current) and excellent noise immunity [3]. The output voltage of the boost PFC converter (the bus voltage) should be always higher than the peak line voltage for an appropriate functioning of the system. For usual line input voltage applications (85 V-265 V rms), the bus voltage is usually fixed to around 400 V DC which is achieved by a voltage feedback compensating loop. In a two-stage power factor correction approach, the first stage PFC boost converter is connected to a second stage buck DC-DC converter (regulating stage) in order to decrease the voltage to a desired value while improving the dynamic performances such as the transient response of the overall system in front of load and line changes. One of the important tasks in the design of PFC power supplies is the control loop implementation with the main aims to achieve a stable system and an adequate dynamic behavior under all loading and power conditions [10]. However, it is well known that stability is difficult to be achieved for all power levels [11]. Recently it was shown through numerical simulations and experimental measurements that boost PFC converter can present period doubling and subharmonic oscillations at the line frequency [11]. This is a very undesirable behavior as it can jeopardize considerably the system performances by increasing its Total Harmonic Distortion (THD). This results in an unacceptable PF value less than 75% which is equal to what it can be obtained from the passive type AC-DC converter composed by a simple bridge rectifier and a bulk capacitor. Realizing the practical importance of PFC AC-DC converters, a series of studies dealing with nonlinear behavior in these systems, have been carried out. We can cite among others the works of Orabi in this field of research [11], [12]. Later, many studies have dealt with period doubling instabilities in boost PFC circuit where bifurcations at both the switching frequency and at line frequency have been studied [13]-[17]. Sub-harmonic and chaotic motions at the line frequency in PFC systems are undesirable and hence control over such phenomena is a topic of considerable interest.

During the two last decades a number of methods have been reported in the literature for controlling chaotic oscillations in nonlinear systems by stabilizing some Unstable Periodic Orbits (UPOs) immersed in the chaotic attractor [18]-[22]. The principle of stabilization is based on perturbation or control by adding an extra input to the nonlinear dynamical system with the aim to modify its dynamic properties by stabilizing the desired behavior. The control input can be either a certain physical action on the system such as a force in a mechanical system or an external voltage in an electrical circuit or either a variation of some parameter of the controlled system in terms of its state variables trajectory in the state space [23]-[25]. Readers interested in a recent and complete classification of chaos control existing methods can consult [19]. One of the most efficient chaos control scheme is the Time Delay Feedback Control (TDFC) first introduced by Pyragas [18] and later applied by many other authors. Roughly speaking, for a nonlinear dynamical system $\dot{x} = f(x(t))$, the time delayed scheme adds a control input $u(t)$ which uses the error between the feedback signal and its τ_d delayed version, *i.e* $u(t) = \eta(y(t-\tau_d) - y(t))$ in such a way that the overall dynamics is described by $\dot{x} = f(x(t)) + \eta(y(t-\tau_d) - y(t))$, where $y(t)$ is a measurable output signal and η is a feedback design parameter. In feedback systems like PFC converters, this input is added in the feedback path. If the time delay τ_d is selected to be the period of the UPO, this can be stabilized by appropriately choosing the time delay feedback gain η. A very important property of this control scheme is that it does not change the periodic orbit of the uncontrolled system. This kind of control scheme is therefore called noninvasive in the sense that the desired behavior of

the system is not modified in contrast to other controllers for which the desired orbit may be altered. PFC converters are characterized by having two forcing periods: the switching period T_s and the line period T_l ($T_l >> T_s$). Many kinds of instabilities can occur at both periods [15]. The first attempt for controlling bifurcation behavior in PFC boost converters is in [9] by using parametric perturbation. Filippov method and the monodromy matrix (see [26]) were used to obtain the stability domain of the controlled system. However, instabilities at the line period have been completely left out. Clearly these instabilities have a stronger effect on the PF than those occurring at the switching period. In [27], it was shown through numerical simulations that the TDFC can be a good solution for stabilizing the boost PFC AC-DC pre-regulator when it is working out of its stability domain. The aim of this work is to study analytically the effect of applying a TDFC to a two-stage PFC AC-DC converter. For this purpose, a Harmonic Balance (HB) approach is used [28]. The rest of the paper is organized as follows: Section 2 will deal with the system description. In Section 3 the nonlinear averaged model of the system is derived by taking into account the TDFC in the voltage loop. Section 4 will be devoted to the analysis of the DC component motion. Conditions for stability are derived by studying the characteristic quasi-polynomial of the τ_d-averaged model. Some bifurcation phenomena of the system are presented in Section 5. In Section 6, dynamic phasor and HB approaches are used to obtain a harmonic model of the system. From a simplified version of this model, conditions for avoiding subharmonic oscillations are derived and the stability domain is located in a suitable design parameter space. Results concerning the stability of the DC component and the first harmonic component are combined in Section 7 to get an overall view of the stability domain of the system. Performances of the proposed control are compared to those of the traditional controller. In the last section, the conclusions of this work are summarized.

2. System Description

2.1. PFC bus voltage control

The schematic diagram of a two-stage PFC AC-DC converter is shown in Fig. 1. Traditionally, with the aim to regulate the bus voltage v of the PFC pre-regulator stage to a desired value V_{ref}, an outer voltage loop controller in the form of a low pass filter is used. In this work , a TDFC is inserted in the output voltage control path in order to control the subharmonic oscillations and the chaotic behavior. With this control unit included, the small signal transfer function of the PFC bus voltage controller can be written in Laplace domain as follows:

$$H_f(s) = \frac{k_o}{1 + s\tau_f}[1 + \eta(\exp(-s\tau_d) - 1)] \tag{1}$$

where $k_o = \frac{R_{vf}}{R_{vi}}$ is the DC gain of the controller, $\tau_f = R_{vf}C_{vf}$ is its time constant, η is the gain of the TDFC and τ_d is its time delay period. The output v_{fb} of the low pass filter is applied to a TDFC block and then a fixed value of 1.5 V is subtracted from this variable to obtain the signal v_{vea} which is used as a conductance emulator that when multiplied by the input voltage, the template of the input reference i_{ref} for the current controller is obtained.

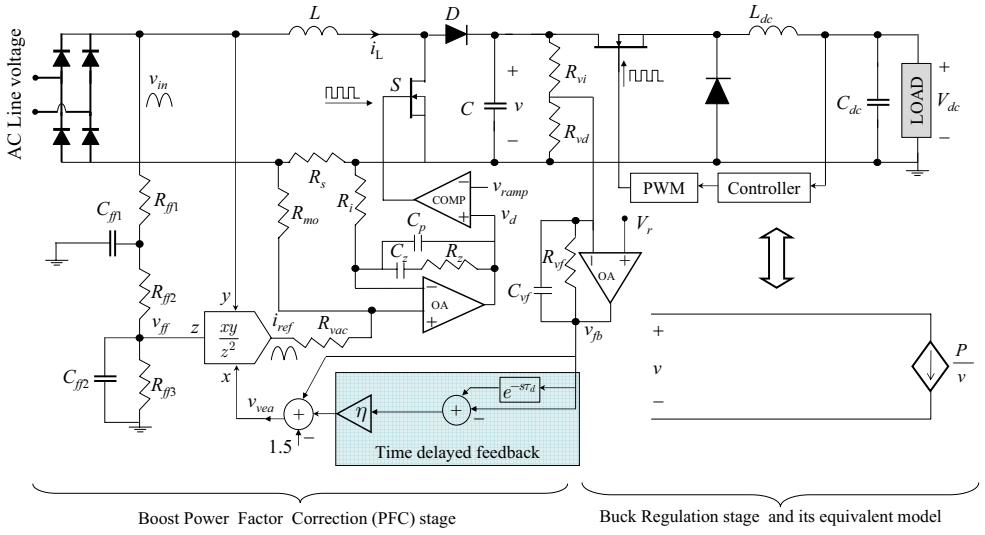

Figure 1. Two-stage PFC AC-DC regulator under fixed frequency average current control.

2.2. Inductor current control

The control of the inductor current is a fundamental task of the overall control system. The main objective of this part of control is to achieve a near unity power factor. For this purpose, the feedback voltage v_{vea} is multiplied by the rectified input sinusoidal voltage $v_{in} = V_{in}|\sin(\omega_l t)|$ and divided by the square of v_{ff}, a measure of the rms value of the input voltage. In this way, the inductor current is programmed to be:

$$i_L(t) = \frac{K}{V_{in}^2} v_{\rm vea} v_{in} \tag{2}$$

where

$$K = \frac{R_{mo} V_{in}}{R_s R_{vac} v_{ff}^2} \tag{3}$$

and V_{in} is the amplitude of the sinusoidal input voltage v_{in}. For (2) to be fulfilled in average, ACM control is used for the inductor current of the boost converter working in CCM.

2.3. Feed-forward Control

The feed-forward control is included in order to take into account changes in the line voltage. The feed-forward voltage v_{ff} is obtained from a second order low pass filter whose DC gain is k_{ff} and whose second order state equation can be written in the following standard form:

$$k_{ff} v_{in} = \frac{d^2 v_{ff}}{dt^2} + 2\zeta_{ff}\omega_{ff}\frac{dv_{ff}}{dt} + \omega_{ff}^2 v_{ff} \tag{4}$$

where k_{ff}, ζ_{ff} and ω_{ff} are the DC gain, the damping coefficient and the natural pulsation of the second order filter that can be obtained easily from the resistances R_{ffk} and the

Table I. Parameter values used in numerical simulations unless otherwise noted. Values not stated here are either stated in the text or in the figure captions.

Parameter	Value	Parameter	Value
V_{in}	$220\sqrt{2}$ V	$\tau_f = \tau_d$	10 ms
$f_l = \frac{1}{T_l}$	50 Hz	k_f	varying
$f_s = \frac{1}{T_s}$	200 kHz	C_p, C_z	62, 620 pF
V_l	1	R_z	18 $k\Omega$
V_u	5.2 V	V_{ff}	$\sqrt{15}$
L	1 mH	V_{ref}	400 V
C	47 μF	R_{vi}	511 $k\Omega$
P	250 W (Full load)	R_{mo}	3.9 $k\Omega$
R_s	0.25 Ω	R_{vac}	910 $k\Omega$

capacitances C_{ffk} (See Fig. 1). It will be supposed that the ripple of the second order filter output is very small in such a way that it can be considered as a purely DC signal ($v_{ff} = V_{ff}$). This condition is easily met in practical design by choosing appropriate values of the filter parameters.

2.4. Pulse width modulator

Power electronics converters work by switching appropriately between different configurations through activating switching devices. In our boost PFC AC-DC converter, the activation of the switch S and the diode D is done in a complementary fashion in such a way that when S is open, D is closed and vice-versa. This is accomplished by using a Pulse Width Modulator (PWM) which works as follows: the inductor current i_L is sensed with a current sensor whose equivalent resistance is R_s, and the current error represented by the difference voltage $R_{mo}i_{\text{ref}} - R_s i_{\text{L}}$ is processed trough the current controller. The output v_d of this controller is connected to the non inverting input of the comparator whereas to the inverting input a T_s-periodic sawtooth ramp signal, whose lower value is V_l and upper value is V_u, is applied in such away that in the steady state the switch is activated each switching cycle while it is turned OFF whenever the ramp voltage $v_{\text{ramp}}(t)$ crosses the control signal v_d.

2.5. Output regulating stage

At the output of the PFC stage, a regulating DC-DC buck converter is connected to decrease the output voltage to a desired value $V_{dc} < V_{ref}$. This stage is separately controlled in such a way that it can be considered as a tightly regulated output voltage V_{dc}. In this case, the DC-DC buck regulating stage can be substituted by a constant power load P (See Fig. 1). As such, provided that the same level of power is used, the same model is obtained for the buck converter operating in both CCM and DCM.

3. A Nonlinear Model for the PFC Converter Under TDFC

Let us consider that the boost pre-regulator is working in CCM. Let us consider also that the inductor current i_L of the first stage and the output voltage V_{dc} of the second stage are tightly controlled to their desired reference. In this case, it can be demonstrated that the T_s-averaged model of the closed loop complete PFC system is given by [11]:

$$v\frac{dv}{dt} = -\frac{P}{C} + \frac{2K}{C}\left(v_{vea}\sin^2(\omega_l t)\right) \tag{5}$$

$$\frac{dv_{fb}}{dt} = \frac{1}{\tau_f}\left(-v_{fb} + k_o\left(\frac{(R_{vd}+R_{vi})V_r}{R_{vd}} - v\right) + V_r\right) \tag{6}$$

where P is the constant power and $v_{vea}(t) = v_{fb}(t) + \eta(v_{fb}(t-\tau_d) - v_{fb}(t))) - 1.5$ is the conductance emulator. Let us write:

$$k_f = Kk_o, V_{ref} = \frac{(R_{vd}+R_{vi})V_r}{R_{vd}}, \quad \text{and} \quad p(t) = K(v_{fb}(t) - 1.5). \tag{7}$$

Therefore the following nonlinear time varying delay differential equations are obtained as a model of the system under the TDFC:

$$\begin{aligned} v\frac{dv}{dt} &= -\frac{P}{C} + \frac{2}{C}[p(t) + \eta(p(t-\tau_d) - p(t))]\sin^2(\omega_l t) \\ \frac{dp}{dt} &= \frac{1}{\tau_f}\left(-p + k_f(V_{ref} - v) + K(V_r - 1.5)\right) \end{aligned} \tag{8}$$

Model (8) is nonlinear and non-autonomous with a forcing frequency $2\omega_l$ and time delay period τ_d. It is worth noting here that in PFC applications, the time delay τ_d must be equal to the period $\frac{T_l}{2}$ of the rectified input voltage in order to stabilize the desired periodic orbit with the same period and therefore to get small THD for the input current. Other values of τ_d may stabilize other unstable periodic orbits with different period than that of the rectified input voltage but these orbits are not of practical use in PFC applications. The approach used in this paper, for analyzing the dynamical behavior of the system and therefore for avoiding undesired behaviors, is based on a separation procedure of the overall dynamics of the system between slow dynamics due mainly to the DC component motion and faster dynamics due to higher harmonic components behavior. First the dynamics of the DC component will be analyzed by using an averaged model over one delay period. Then, the dynamics of the harmonics responsible for the first period doubling are analyzed by using a dynamic phasor approach.

4. Study of the Stability of the DC component motion

4.1. Averaged model over one delay period

By carrying out a time averaging of (8) over one time delay period τ_d, the following τ_d-averaged model is obtained:

$$\begin{aligned} v_0\frac{dv_0}{dt} &= \frac{1}{C}(p_0(t) + \eta(p_0(t-\tau_d) - p_0(t)) - P) \\ \frac{dp_0}{dt} &= \frac{1}{\tau_f}\left(-p_0 + k_f(V_{ref} - v_0) + K(V_r - 1.5)\right) \end{aligned} \tag{9}$$

where v_0 and p_0 are the τ_d-averaged state variables given by:

$$\begin{array}{l} v_0 = \int_{t-\tau_d}^{t} v(\tau)d\tau \\ p_0 = \int_{t-\tau_d}^{t} p(\tau)d\tau \end{array} \tag{10}$$

The equilibrium point of this nonlinear averaged model is given by:

$$\begin{array}{l} V_0 = V_{ref} + \dfrac{K(V_r - 1.5) - P}{k_f} \\ P_0 = P \end{array} \tag{11}$$

Let us consider that the DC component x_0 of a state variable x can be expressed as the sum of the steady state value X_0 and a small disturbance $\tilde{x}_0$ ($v_0 = V_0 + \tilde{v}_0$ and $p_0 = P_0 + \tilde{p}_0$). By performing a linearization in the vicinity of the equilibrium point $X_0 = (V_0, P_0)^t$, the following linear time delay model is obtained:

$$\begin{array}{l} \dfrac{d\tilde{v}_0}{dt} = \dfrac{1}{V_0 C}(\tilde{p}_0(t) - \eta(\tilde{p}_0(t-\tau_d) - \tilde{p}_0(t)) \\ \dfrac{d\tilde{p}_0}{dt} = \dfrac{1}{\tau_f}\left(-k_f\tilde{v}_0 - \tilde{p}_0\right) \end{array} \tag{12}$$

For an ordinary differential equation, the stability can be studied by the characteristic polynomial of the linearized system. However (12) is a delay differential equation characterized by a quasi-polynomial [29]. The quasi-polynomial of (12) is given by:

$$\det(\mathbf{J}_0 + \mathbf{J}_{\tau_d}\exp(-s\tau_d) - s\mathbb{I}) \tag{13}$$

where $\mathbb{I}$ is 2×2 unity matrix, $\mathbf{J}_0$ is the Jacobian matrix with respect to the non-delayed states and $\mathbf{J}_{\tau_d}$ is the Jacobian matrix with respect to the delayed states. These Jacobian matrices are given by:

$$\mathbf{J}_0 = \begin{pmatrix} 0 & \dfrac{1-\eta}{V_o C} \\ -\dfrac{k_f}{\tau_f} & -\dfrac{1}{\tau_f} \end{pmatrix}, \ \mathbf{J}_{\tau_d} = \begin{pmatrix} 0 & \dfrac{\eta}{V_o C} \\ 0 & 0 \end{pmatrix} \tag{14}$$

By expanding (13), the following characteristic quasi-polynomial equation is obtained:

$$s^2 + \frac{1}{\tau_f}s + \frac{k_f}{V_0 C \tau_f}[1 + \eta(\exp(-s\tau_d) - 1)] = 0 \tag{15}$$

To determine the local stability of the equilibrium point, we first consider the solution of (15) which is transcendental and has an infinite number of roots for every set of fixed parameter values. The equilibrium point is locally stable if all these roots have negative real part. At a bifurcation point, a root s_0 of (15) can be written as $s_0 = 0 + j\Omega_0$. Substituting in (15) yields:

$$-\Omega_0^2 + \frac{1}{\tau_f}j\Omega_0 + \frac{k_f}{V_0 C \tau_f}[1 + \eta(\exp(-j\Omega_0\tau_d) - 1)] = 0 \tag{16}$$

Separating the real and the imaginary parts gives:

$$\begin{array}{l} -\Omega_0^2 + \dfrac{k_f}{V_0 C} + \dfrac{k_f \eta}{V_0 C \tau_f}(\cos(\Omega_0\tau_d) - 1) = 0 \\ \dfrac{\Omega_0}{\tau_f} - \dfrac{k_f \eta}{V_0 C \tau_f}\sin(\Omega_0\tau_d) = 0 \end{array} \tag{17}$$

Note that this set of equations is unchanged under the transformation of $\Omega_0 \to -\Omega_0$ and that $\Omega_0 = 0$ is not a solution whenever $k_f > 0$ and therefore, the unique possible singularity for the DC component is a Hopf bifurcation. This implies that a pair or pairs of complex conjugate roots will cross the imaginary axis when the bifurcation parameter reaches a critical value. Solving (17) for k_f yields:

$$\begin{aligned} k_{f,dc,1} &= \frac{\Omega_0^2 V_0 C \tau_f}{1 + \eta\cos(\Omega_0\tau_d) - \eta} \\ k_{f,dc,2} &= \frac{\Omega_0 V_0 C}{\eta \sin(\Omega_0 \tau_d)} \end{aligned} \tag{18}$$

One way to visualize the solution of (16) is to seek graphically for values Ω_0 satisfying (17) in a 2-dimensional plane. In Fig. 2, the evolution of $k_{f,dc,1}$ and $k_{f,dc,2}$ is depicted in terms of Ω_0 for different values of η. For $\eta = 0$, the curve $k_{f,dc,2}$ does not exist meaning that no solution is possible for Ω_0, a result that can be readily obtained from (17). For $\eta = 0.2$, both curves exist but they do not intersect meaning that no solution is possible for Ω_0. For $\eta = 0.3$, the curves intersect in two points and therefore two solutions for Ω_0 exists. In this case, it is expected that the DC component will oscillate at these frequencies when the parameter k_f is equal to the critical values $k_{f,dc,1}$ and $k_{f,dc,2}$.

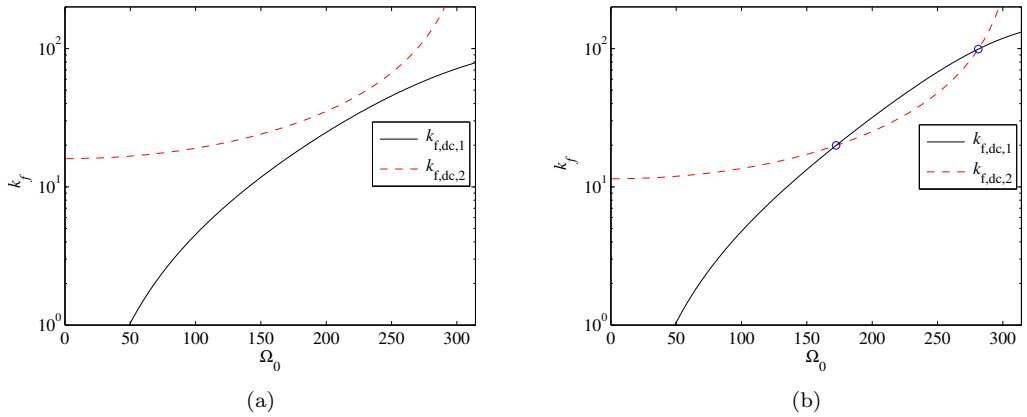

Figure 2. Boundary curves $k_{f,dc,1}$ and $k_{f,dc,2}$ in terms of Ω_0 in the interval $(0, \frac{\pi}{\tau_d})$. (a) $\eta = 0.25$: The curves do not intersect and no solution for Ω_0 exist. (b) $\eta = 0.35$: The curves intersect at the points (172.42, 19.94) and (281.15, 99.15) indicated by a circle. Two solutions exist for Ω_0 and it is expected that the DC component will oscillate at these frequencies.

4.2. Approximate analytic solution for the characteristic quasi-polynomial

Although (17) can be used to obtain numerically the critical value of the parameters, it is more useful to have an explicit expression for the stability boundaries. For many application the feedback gain k_f and the delay gain η are design parameters that should be adjusted accordingly to the values of other parameters. Our purpose in this paper is to perform an analytical study by carrying out some realistic approximations. Unfortunately, there is no

universal procedure to obtain approximately the boundary curves. In this work the second order PadÃ© approximation ([30]) will be used in order to get a closed form expression for the stability of the DC component motion. By performing a second order PadÃ© approximation for the delay transfer function $\exp(-s\tau_d)$, (15) can be written as follows:

$$\alpha_4 s^4 + \alpha_3 s^3 + \alpha_2 s^2 + \alpha_1 s^1 + \alpha_0 \tag{19}$$

where

$$\begin{aligned} \alpha_4 &= V_0 C \tau_d^2 \tau_f \\ \alpha_3 &= 6V_0 C \tau_d \tau_f + V_0 C \tau_d^2 \\ \alpha_2 &= 12V_0 C \tau_f + k_f \tau_d^2 + 6V_0 C \tau_d \\ \alpha_1 &= 12V_0 C + 6k_f \tau_d - 12k_f \eta \tau_d \\ \alpha_0 &= 12k_f \end{aligned} \tag{20}$$

By applying the Routh-Hurwitz criterion ([30]) to (19), the following expression for the critical value of the time delay feedback gain η is obtained:

$$\eta_{dc} = \frac{1}{4} - \frac{6V_0 C(4\tau_d\tau_f + 12\tau_f^2 + \tau_d^2) - k_f\tau_d^3 + \sqrt{sq_1}}{24k_f\tau_d^2\tau_f} \tag{21}$$

where

$$\begin{aligned} sq_1 = {} & V_0^2 C^2(576\tau_d^3\tau_f + 3168\tau_d^2\tau_f^2 + 5184\tau_f^4 + 36\tau_d^4 + 6912\tau_d\tau_f^3) + k_f^2(\tau_d^6 + 36\tau_d^4\tau_f^2 + 12\tau_d^5\tau_f) \\ & -V_0 C(864k_f\tau_d^2\tau_f^3 - 120k_f\tau_d^4\tau_f - 12k_f\tau_d^5 - 144k_f\tau_d^3\tau_f^2) \end{aligned} \tag{22}$$

η_{dc} gives the critical value of the time delay feedback gain η beyond which, the stability of the DC component motion is lost. If $\eta > \eta_{dc}$, two roots of the characteristic equation (19) are complex conjugates with positive real parts. Therefore the DC component presents slow oscillations making the complete forced system to exhibit quasi-periodic behavior and phase-locked orbits. If $\eta < \eta_{dc}$, all the roots of (19) are in the left half plane of the complex domain and therefore the DC component converges to the equilibrium point (V_0, P_0). Figure 3 shows η_{dc} in terms of k_f obtained both analytically using (21) and numerically using (18). It can be observed that the PadÃ© approximation gives a very accurate stability boundary.

So far we have considered the dynamics of the DC component. However, the previous analysis does not provide any information about the other components of the harmonic model. In Section 6 a dynamical analysis of the first harmonic model under the TDFC will be carried out. It will be shown that this model has the origin as an equilibrium point. If this equilibrium point is stabilized, subharmonic and chaotic oscillations can be removed.

5. Bifurcation Behavior of the Free System

Let us first explore the possible dynamics of the system without considering TDFC ($\eta = 0$). Figure 4(a) shows the bifurcation diagram of the system taking the total feedback gain k_f as bifurcation parameter. The THD of the input current i_{in} is shown in Fig. 4(b) as the bifurcation parameter is varied. The THD for a variable x over one period $\frac{2\pi}{\omega_0}$, is defined as follows:

$$\text{THD} = 100\frac{\sqrt{X_{\text{rms}}^2 - X_{\omega_0}^2 - X_0^2}}{X_{\omega_0}} \tag{23}$$

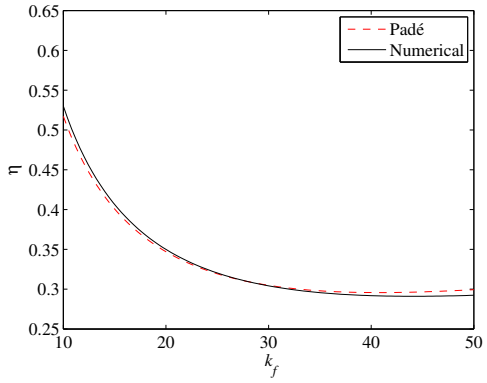

Figure 3. Boundary curves in the plane (k_f, η) obtained analytically using the PadÃ© approximation and by solving numerically (18) using Newton Raphson algorithm.

where X_{rms} is the overall rms value of the variable x, X_{ω_0} is its fundamental component and X_0 is the DC component. A period doubling route to chaos can be clearly observed in the figure when k_f is increased. It can be noted that the first bifurcation takes place at a value of $k_f \approx 32$. This result will be confirmed analytically by analyzing the dynamics of the first harmonic component. The analytically calculated equilibrium point V_0 of Eq. (11) is also depicted in Fig. 4(a) in dashed line showing a good agreement with the result obtained from computer simulation.

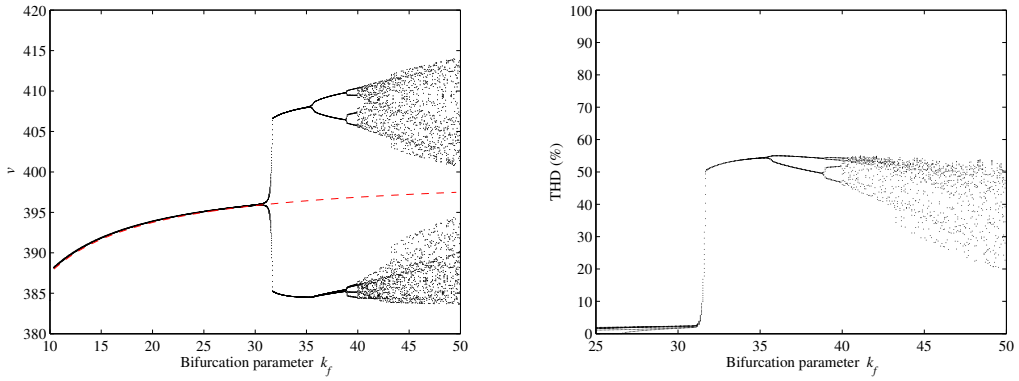

(a) (b)

Figure 4. Bifurcation diagram of the AC-DC PFC converter by taking the feedback gain k_f as a bifurcation parameter showing a period doubling route to chaos. (a) Bifurcation diagram depicting the $\frac{T_l}{2}$-sampled PFC output voltage v. The equilibrium point V_0 is also shown in dashed line. (b) THD of the input current i_{in} showing a significant increasing the THD after the first bifurcation takes place.

Time domain waveforms and the FFT spectra of the bus voltage are shown in Fig. 5(a). It can

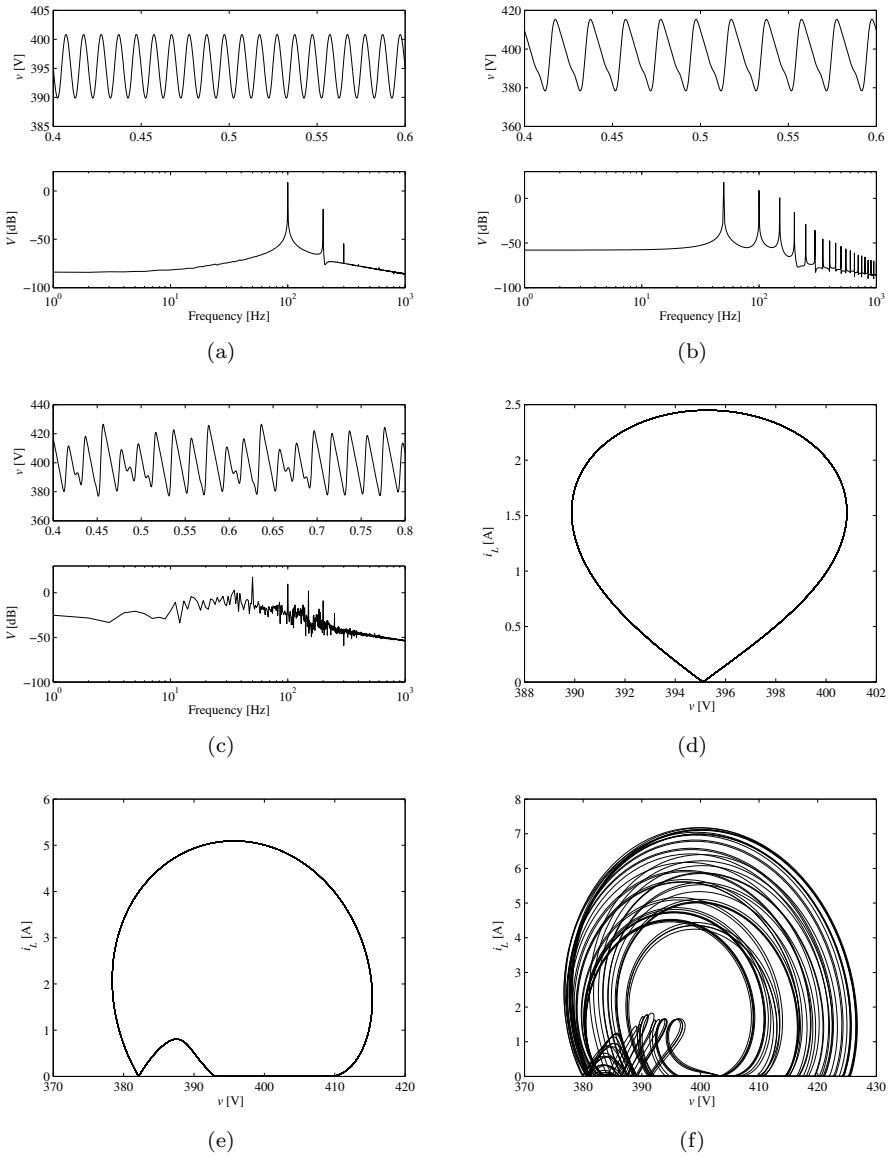

Figure 5. Time domain waveforms and FFT spectra of the bus voltage and state plane trajectories in the $(v,\, i_L)$ plane showing different dynamic behaviors of the AC-DC PFC converter. (a) (d) $k_f = 25$: normal periodic behavior. (b), (e) $k_f = 32$: subharmonic oscillations. (c), (f) $k_f = 50$: chaotic regime.

be clearly seen that in the periodic regime a dominant spike at $2f_l$ (100 Hz) exists. Some small spikes at $4f_l$ and at $6f_l$ can also be observed but they can be neglected. For the subharmonic regime, there is a dominant spike at f_l and its integer multiple causing subharmonic oscillation. In the chaotic regime there is a continuous spectrum between zero and about $4f_l$ but the spikes

at f_l and its harmonics are clearly dominant. Trajectories of the system in (v, i_L) state plane are also shown. Periodic orbit, subharmonic motion and chaotic attractor for different values of the feedback gain k_f are depicted in Fig. 5(d)-5(f).

6. Dynamic Phasor-Based Harmonic Averaged Model

Although the averaged model (8) is enough accurate to get numerical simulations like those presented in Section 3, it is not possible to derive from this model analytical expressions for other asymptotic stability boundaries rather than the slow oscillations of the DC component model. Such expressions will be obtained by performing a HB and studying the stability of the first order harmonics. The approach is based on using time varying (dynamic) Fourier coefficients for the state variables and performing a HB for each frequency. Then harmonics of interest are studied using well known techniques in time domain. Being the PFC converter an excited nonlinear system, the state variables may have a period equal to a multiple integer of the period of the external excitation. The excitation period for the PFC AC-DC converter is $\frac{T_l}{2}$. Consequently, at the first period doubling point, the state variables contain frequency components at the line frequency f_l and its harmonics. The key idea is that a time-domain waveform $x(t)$ can be represented on the interval $(t - T_l, t)$ using a Fourier series with time varying coefficients. Performing a Fourier analysis of the state variables up to Nth order we can write for a state variable $x(t)$:

$$x(t) \approx \sum_{k=-N}^{N} x_k(t) \exp(jk\omega_l t) \tag{24}$$

$$\tag{25}$$

where N is the number of terms (order of the harmonic model) which depends on the accuracy required and $x_k(t)$ is the dynamic time varying Fourier coefficient (k-th dynamic phasor) for the state variable x given by:

$$x_k(t) = \frac{\omega_l}{2\pi} \int_{t-T_l}^{t} x(\tau) \exp(-jk\omega_l \tau) d\tau \tag{26}$$

Note that the dynamic phasor approach requires that the Fourier coefficients describing the waveforms of interest to be sufficiently slow. Then, we can obtain a state-space model in which the Fourier coefficients are the state variables and their stability will determine the stability of the system. Let $\mathrm{v} = [v_{-N} \ \ldots \ v_0 \ \ldots \ v_N]$, $\mathrm{e} = [e_{-N} \ \ldots \ e_0 \ \ \ldots \ \ e_N]^T$ and $e_k = \exp(jk\omega_l t)$. Therefore it can be written: $v(t) \approx \mathrm{v} \cdot \mathrm{e}$, $p(t) \approx \mathrm{p} \cdot \mathrm{e}$, $\sin(\omega_l t) = \mathrm{s} \cdot \mathrm{e}$, $\mathrm{s} = [0 \ \ldots \ -\frac{j}{2} \ \ 0 \ \ \frac{j}{2} \ \ldots \ 0]$, $\delta p(t) = \eta(p(t-\tau_d) - p(t))$. By substituting these expressions in (8), the following N-th harmonic nonlinear model is obtained:

$$\begin{aligned} \mathrm{v} \cdot \mathrm{e} \left(\frac{d\mathrm{v}}{dt} \cdot \mathrm{e} + \mathrm{v} \cdot \frac{d\mathrm{e}}{dt} \right) &= -\frac{(\mathrm{v} \cdot \mathrm{e})^2}{RC} + \frac{2}{C} \left((\mathrm{p} + \delta \mathrm{p}) \cdot \mathrm{e} \right) (\mathrm{s} \cdot \mathrm{e})^2 \\ \frac{d\mathrm{p}}{dt} \cdot \mathrm{e} + \mathrm{p} \cdot \frac{d\mathrm{e}}{dt} &= \frac{1}{\tau_f} \left(-\mathrm{p} \cdot \mathrm{e} + k_f \left(V_{ref} - \mathrm{v} \cdot \mathrm{e} \right) \right) \end{aligned} \tag{27}$$

where

$$\begin{array}{l} \dfrac{d\mathrm{e}}{dt} = [-j\omega_l N e_{-N} \ \ldots \ e_0 \ \ldots \ j\omega_l N e_N] \\ \dfrac{d\mathrm{v}}{dt} = \left[\dfrac{dv_{-N}}{dt} \ldots \dfrac{dv_0}{dt} \ldots \dfrac{dv_N}{dt}\right] \\ \dfrac{d\mathrm{p}}{dt} = \left[\dfrac{dp_{-N}}{dt} \ldots \dfrac{dp_0}{dt} \ldots \dfrac{dp_N}{dt}\right] \end{array} \tag{28}$$

6.1. Some basic properties

Three basic key properties are used to develop the harmonic dynamical model.

Property 1. *The time derivative of the k-th phasor is given by the following expression:*

$$\frac{dx_k}{dt} = \left[\frac{dx}{dt}\right]_k - jk\omega_l x_k \tag{29}$$

Property 2. *The k-th phasor of a product of two time-domain variables is equal to the discrete-time convolution of the corresponding phasor sets of each component.*

$$[xy]_k(t) = \sum_{n=-\infty}^{\infty} y_n x_{k-n} \tag{30}$$

Property 3. *The k-th phasor of a delayed version of a time-domain variable is equal to the corresponding phasor of the non-delayed variable multiplied by* $\exp(-jk\omega_l\tau_d)$*,* i.e*:*

$$[x(t-\tau_d)]_k(t) = x_k(t)\exp(-jk\omega_l\tau_d) \tag{31}$$

It should be noted also that since all state variables are real we have that $x_k = x_k^*$, where * stands for the complex conjugate operator.

6.2. First order harmonic model

Our aim in this section is to derive simple nonlinear model governing the amplitude of oscillations in the vicinity of the bifurcation boundary where high harmonics amplitudes are small and their corresponding nonlinearities are weak. From the spectra presented in Figures 5(a)-5(c), it can be observed that harmonics of order bigger than 2 can be neglected. This observation together with some assumptions will be used in this work. If $N = 2$ is chosen and the first harmonic component equations are isolated from the full order harmonic model, the following nonlinear model is obtained:

$$\frac{d}{dt}(v_0 v_1 + v_2 v_1^*) = -j\omega_l(v_0 v_1 + v_2 v_1^*) + \frac{1}{2C}(2p_1 - p_1^*)(1-2\eta) \tag{32}$$

$$\frac{dp_1}{dt} = -\frac{1}{\tau_f}(j\omega_l\tau_f + 1)p_1 - \frac{k_f}{\tau_f}v_1 \tag{33}$$

This is a nonlinear model in the complex domain with two complex state variables v_1 and p_1 making its stability analysis a challenging task. Higher order harmonic analysis approximation can provide much more accurate results away from the critical bifurcation points and ever can predict more complex nonlinear phenomena such as possible coexisting attractors. However, it is very interesting from a practical point of view to be able to derive analytical expressions of

the critical boundaries corresponding to the first period doubling bifurcation. These expressions become transcendental with high order approximations. For this reason, our analysis is restricted to second order HB approximation. Then, the dynamic behavior of the first order component is used to predict the subharmonic oscillations of the system by considering that the DC component and the second order harmonics are practically constant ($v_2 = V_2$ and $v_0 = V_0$). This is a practical approach since the subharmonic instability is mainly due to the appearance of a non zero first order component.

7. Stability Domain

7.1. Some practical assumptions

Let v_1 be the first harmonic component of the state variable v and V_0 and V_2 be its DC and second harmonic components at the steady state. By performing a circuit theory analysis on the controlled system at steady state, we obtain $V_2 = \rho V_0 \exp(j\varphi_2)$, where for a practical two-stage PFC AC-DC converter

$$\rho \approx \frac{V_0}{4PC\omega_l}, \quad \varphi_2 = \pi - \tan^{-1}\left(\frac{1}{2\rho}\right) \tag{34}$$

Note that ρ stands for the relative ripple of the PFC converter output voltage and therefore it is a parameter that should be taken into account in a practical design. A system with relatively appreciable voltage ripple in the bus voltage feedback loop will lead a fast transient response as stated in [31].

7.2. Stability of the first harmonic component motion

By writing v_1 and p_1 in cartesian form ($v_1 = \Re(v_1) + j\Im(v_1)$ and $p_1 = \Re(p_1) + j\Im(p_1)$) and substituting in (32)-(33), the linear equations describing the first order dynamic phasor motion are obtained:

$$\dot{\zeta} = \mathbf{J}\zeta \tag{35}$$

where the harmonic state vector written in cartesian form is

$$\zeta = \begin{pmatrix} \Re(v_1) \\ \Im(v_1) \\ \Re(p_1) \\ \Im(p_1) \end{pmatrix} \tag{36}$$

and the matrix $\mathbf{J}$ is given by:

$$\mathbf{J} = \begin{pmatrix} 0 & \dfrac{\omega_l \check{V}}{\hat{V}} & \dfrac{1-2\eta}{2C\hat{V}} & 0 \\ -\dfrac{\omega_l \hat{V}}{\check{V}} & 0 & 0 & \dfrac{3(1-2\eta)}{2C\check{V}} \\ -\dfrac{k_f}{\tau_f} & 0 & -\dfrac{1}{\tau_f} & \omega_l \\ 0 & -\dfrac{k_f}{\tau_f} & -\omega_l & -\dfrac{k_f}{\tau_f} \end{pmatrix} \tag{37}$$

where $\check{V} = V_0 - |V_2| = V_0(1-\rho)$ and $\hat{V} = V_0 + |V_2| = V_0(1+\rho)$ are the maximum and the minimum values of the pre-regulator output voltage v respectively.

7.3. Stability boundaries

It can be observed from (35) that the equilibrium point of the first order harmonic model is the origin. The study of its stability can be performed by using the eigenvalues of the matrix $\mathbf{J}$. If all eigenvalues have negative real part, then the origin is stable. If an eigenvalue has positive real part, then this equilibrium point is unstable and subharmonic oscillations will appear in the nonlinear system. The first order harmonic component will reach a new non-zero equilibrium point whose value will depend on the dynamics of other harmonics not considered in this analysis. To find the stability boundary, the value of parameters at which there is a sudden change in the stability of the equilibrium point are obtained. Mathematically, when an equilibrium point looses stability, an eigenvalue or a complex conjugate pair of eigenvalues of the Jacobian matrix crosses the imaginary axis. The eigenvalues of the matrix $\mathbf{J}$ can be obtained from the equation $\det(\mathbf{J} - \lambda\mathbb{I}) = 0$ which gives the following characteristic polynomial equation:

$$\lambda^4 + \frac{2}{\tau_f}\lambda^3 + a_2\lambda^2 + a_1\lambda + a_0 = 0 \tag{38}$$

where coefficients a_2, a_1 and a_0 are given by:

$$\begin{aligned}
a_2 &= \frac{2k_f(1-\eta)\tau_f(\hat{V}+3\check{V}) + 4C\hat{V}\check{V}(1+2(\omega_l\tau_f)^2)}{\tau_f^2 C\hat{V}\check{V}},\\
a_1 &= \frac{k_f(1-\eta)(3\hat{V}+\check{V}) + 4\omega_l^2 C\hat{V}\check{V}\tau_f}{2\tau_f^2 C\hat{V}\check{V}},\\
a_0 &= \frac{-2\omega_l^2 C\tau_f k_f(1-\eta)(\hat{V}+3\check{V}) + 3(k_f(1-\eta))^2 + (2\omega_l C)^2\hat{V}\check{V}(1+\omega_l^2\tau_f^2)}{(2\tau_f C)^2\hat{V}\check{V}}
\end{aligned} \tag{39}$$

By simply solving Eq. (38), the eigenvalues of the matrix $\mathbf{J}$ can be derived.

Remark 1.

A careful examination of the characteristic polynomial, reveals that for values of k_f lower than a first critical value, the first eigenvalue corresponds to a stable mode with a very large time constant. For the case studied in this work, this mode can sometimes be unstable. The second eigenvalue corresponds to a stable mode with a very small time constant. Thus, a perturbation in the direction of its eigenvector will be quickly damped.

Remark 2. *The third and fourth eigenvalues correspond to stable complex conjugate modes. Analysis of the associated eigenvector indicates that these modes introduces an oscillatory motion but as if it is quickly damped, it is not noted in the waveforms of the system. However if these oscillations are not sufficiently damped, low frequency oscillations, at a frequency larger than the line period, will manifest its self in the waveforms of the system.*

Remark 3. *For values of k_f larger than a second critical value, all eigenvalues become complex and stable. The motion in the vicinity of the equilibrium point exhibits under damped oscillation.*

Figure 6 shows the trajectories of the first order component for different cases. For the stable case, the trajectories converge to the origin after some transients while for the unstable case, the origin is a repeller and trajectories are attracted by an attractor equilibrium point which depends on the dynamics of other harmonics not considered in this analysis.

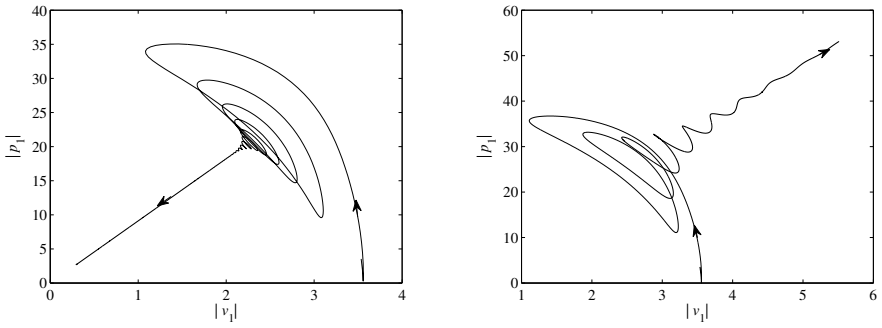

(a) (b)

Figure 6. Dynamics of the first harmonics components for different values of k_f. (a) $k_f = 30$: the origin is stable characterized by two stable complex conjugate eigenvalues $\lambda_{1,2} = -50.00 \pm 586.38j$ and two stable real eigenvalues $\lambda_{3,4} = (-1.42, -98.57)$ (b) $k_f = 32$: the origin is unstable with two stable complex conjugate eigenvalues $\lambda_{1,2} = -50.00 \pm 595.77j$, two real, one stable ($\lambda_3 = -109.30$), and one unstable ($\lambda_4 = 9.30$) eigenvalues.

Instead of finding explicitly the eigenvalues of $\mathbf{J}$, the location the stability boundary can be computed by applying the Routh Hurwitz criterion to the characteristic equation of the matrix $\mathbf{J}$. By applying this criterion, the following expressions for the critical values of the time delay feedback gain η is obtained:

$$\begin{aligned}
8\eta_{cri,1} &= \frac{k_f\tau_f(3\hat{V}+\check{V}) + 4C\hat{V}\check{V}(1+(\omega_l\tau_f)^2)}{2k_f\tau_f(3\hat{V}+\check{V})}, \qquad \eta_{cri,2} = \frac{1}{2},\\
\eta_{cri,3} &= \frac{32\hat{V}^2\check{V}(\tau_f\omega_l)^2C + k_f\tau_f((3\hat{V})^2 - 6\hat{V}\check{V})}{2k_f\tau_f((3\hat{V}-\check{V})^2},\\
\eta_{cri,4} &= \frac{1}{2k_f}(k_f - (\frac{\hat{V}}{3}+\check{V})\omega_l^2C\tau_f + \frac{\sqrt{sq_2}}{3}),\\
\eta_{cri,5} &= \frac{1}{2k_f}(k_f - (\frac{\hat{V}}{3}+\check{V})\omega_l^2C\tau_f - \frac{\sqrt{sq_2}}{3})
\end{aligned} \tag{40}$$

By studying the expressions of these critical values, the stability domain can be obtained. Note that $\eta_{cri,4}$ and $\eta_{cri,5}$ has a physical meaning only if sq_2 is positive, where sq_2 is given by:

$$sq_2 = (\omega_l^2C\tau_f)^2(3\check{V}-\hat{V})^2 - 12(\omega_lC)^2\hat{V}\check{V} \tag{41}$$

The critical value $\tau_{f,cri}$ of τ_f giving positive values of sq_2, and therefore real solution for $\eta_{cri,4}$ and $\eta_{cri,5}$ is:

$$\tau_{f,cri} = \frac{2\sqrt{3\hat{V}\check{V}}}{\omega_l|\hat{V}-3\check{V}|} \tag{42}$$

Remark 4. *If $\tau_f > \tau_{f,cri}$, both boundaries corresponding to $\eta_{cri,4}$ and $\eta_{cri,5}$ are real. At $\tau_f = \tau_{f,cri}$, they coalesce and disappear.*

Remark 5. *It can be remarked that $\frac{1}{2} < \eta_{cri,3} < \eta_{cri,1}$ and the boundaries corresponding to $\eta_{cri,1}$ and $\eta_{cri,3}$ can be omitted. Also when $\eta_{cri,4}$ and $\eta_{cri,5}$ exist ($sq_2 > 0$), $\eta_{cri,5} < \eta_{cri,4}$ and therefore $\eta_{cri,5}$ can also be discarded.*

All the previous expressions and inequalities can be used to plot the stability domain and to give the value of η for a successful TDFC. The stabilization of the system will be successful if the time delay feedback gain η is selected in such a way that both the DC and the first harmonic components are stable:

$$\eta_{cri,4} < \eta < \min\left(\eta_{dc}, \frac{1}{2}\right) \tag{43}$$

where η_{dc} is given by Eq. (21). In Figure 7, the stability domain is presented in the (k_f, η) parameter space for a value of $\tau_f > \tau_{fcri}$ which is the case in practice. Possible dynamical behaviors are indicated in their corresponding areas by different colors. The stable domain is

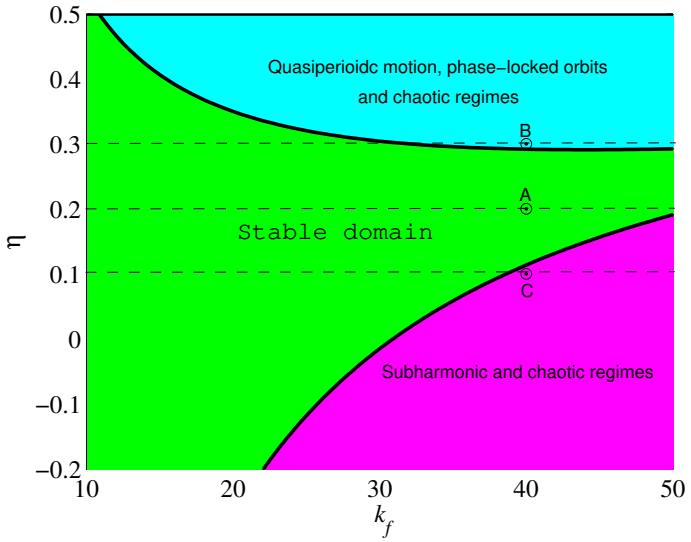

Figure 7. Stability domain in the parameter space (k_f, η).

plotted in green color. In this region both the DC component dynamics and the first harmonic component are stable and therefore the system presents periodic behavior at twice the line frequency as it is desired in a practical application. For relatively high values of η the DC component may lose its stability. A low frequency oscillation is then generated like in a Hopf bifurcation that when it is superimposed to the forced oscillations, the system exhibits quasi-periodic oscillations and phase-locked orbits due to synchronization phenomena. For values of $\eta < \eta_{dc}$, the DC component is stable for whatever feedback gain k_f. However, the zero first

harmonic component can loose its stability at critical values of k_f giving rise to subharmonic oscillations and chaotic behavior. In order to check the correctness of the analytically obtained boundaries, numerical simulations using Feigenbaum diagrams are produced for different values of the TDFC parameter η (corresponding to dashed lines in Fig. 7). The results are shown in Fig. 8. It can be observed that these numerically obtained Feigenbaum diagrams are in good agreement with the derived analytical results plotted in Fig. 7. Figure 9 shows the time domain

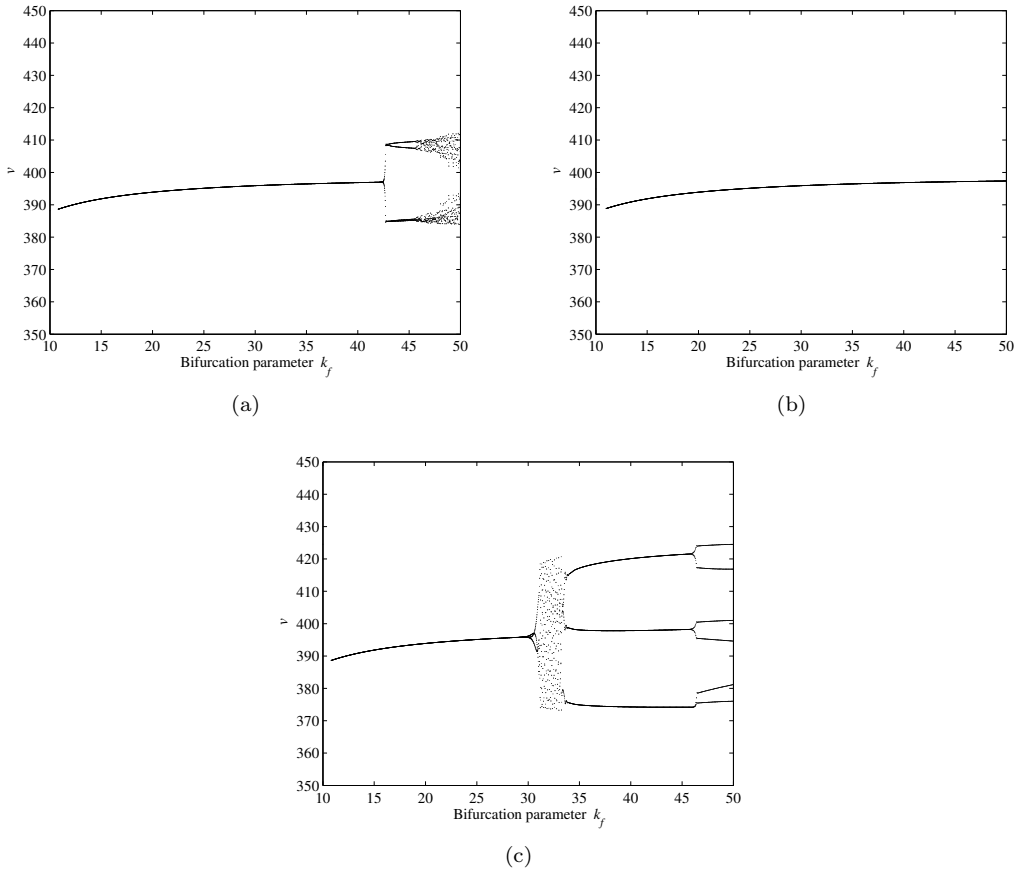

Figure 8. Bifurcation diagrams taking k_f as a bifurcation parameter and η as a secondary bifurcation parameter showing different scenarios of losing stability of the main periodic orbit. (a) $\eta = 0.1$: period doubling bifurcation and its associated route to chaos. The first period doubling is delayed with respect to the system without TDFC. (b) $\eta = 0.2$: the system stabilization is successful for the whole range of k_f. (c) $\eta = 0.3$: excessive value of η can destabilize the DC component causing Hopf bifurcation and quasi-periodic behavior.

waveforms of the output voltage and the control signal δp when the TDFC is activated. Three different values of η were used, one value within the stability domain and therefore the TDFC is successful (Point A in Fig. 7), two values outside the stability domain being the action of the TDFC unsuccessful (Points B and C in Fig. 7). It can be noted that, in the successful case,

and a consequence of the non-invasiveness feature of the TDFC, the control effort is zero once the periodic orbit is stabilized. In Fig. 9(c) (Point B in Fig. 7), the TDFC gain is excessive and in this case the DC component looses stability through a Hopf bifurcation making the overall behavior quasi-periodic. The incommensurate frequencies of this quasi-periodic behavior may synchronize to give rise to phase-locked orbits. Also, the quasi-periodic attractor may loose stability via torus breakdown leading to chaotic regimes.

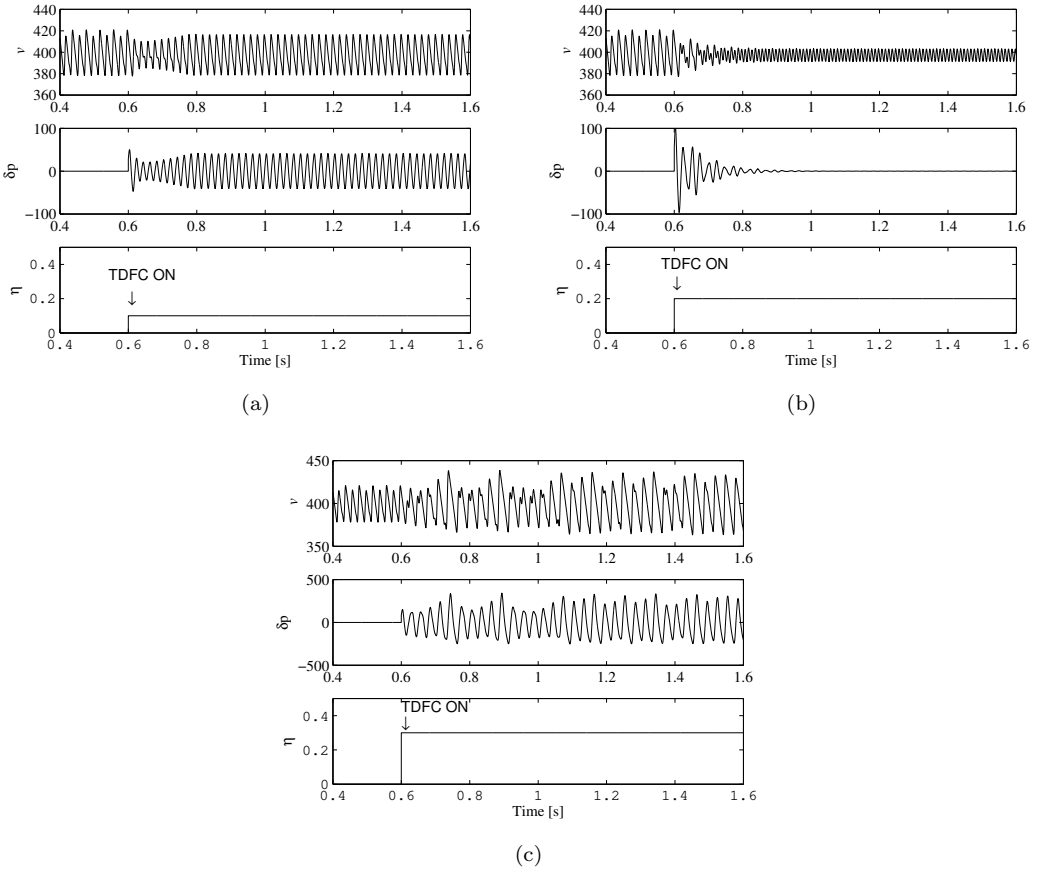

Figure 9. Time domain responses of the output voltage, the control signal by activating the TDFC. (a) $\eta = 0.1$: outside the stability domain (Point C in Fig. 7) implying an unsuccessful TDFC. (b) $\eta = 0.2$: within the stability domain (Point A in Fig. 7) and the control signal δp converges to zero being the TDFC successful. (c) $\eta = 0.3$: outside the stability domain (Point B in Fig. 7) implying an unsuccessful TDFC. $k_f = 40$.

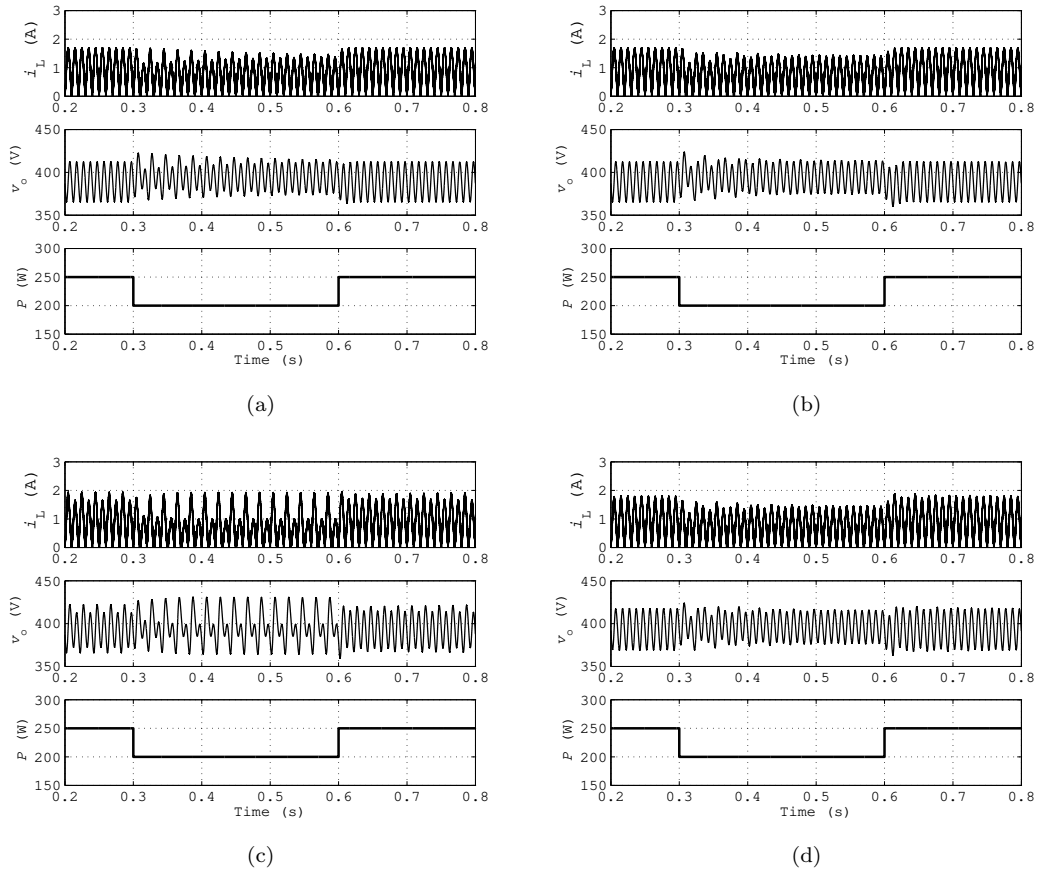

Figure 10. Time domain responses of the rectified input current and the pre-regulator output voltage for step changes of the power level and for different feedback gains. (a) without TDFC $\eta = 0$ and $k_f = 36$: The steady state THD is about 2%. (b) with TDFC $\eta = 0.25$ and $k_f = 36$: The steady state THD is about 2%. (c) without TDFC $\eta = 0$ and $k_f = 40$. The THD is about 10% for $P = 250$ W and about 50% for $P = 200$ W. (d) with TDFC $\eta = 0.25$ and $k_f = 40$. The steady state THD is about 2% for both $P = 250$ W and $P = 200$ W.

7.4. TDFC performances in front of load changes

The performances of the PFC AC-DC two stage regulator with the proposed TDFC is compared to those of the same system without TDFC. Both systems are supplied by a 50 Hz input voltage of 220 V rms. Other parameters are those shown in Table I. At nominal operating conditions, the boost PFC converter switches at 200 kHz and supplies 250 W to its 400 V DC output. The performances have been verified through simulation using PSIM package. The rectified input current, the power level and the output voltage are shown in Fig. 10. This figure shows the dynamic response of the system, when there is step change in load from 250 W (full load) to 200 W (80% load) and vice-versa. As it can be observed, the

Table II. Comparison between performances of the system with and without TDFC for a power level $P = 200$ W.

System Controller	PF	THD	t_s
Proposed (TDFC) ($\eta = 0.25$, $k_f = 36$)	0.99	2%	125 ms
Conventional ($\eta = 0$, $k_f = 36$)	0.99	2%	300 ms
Proposed (TDFC) ($\eta = 0.25$, $k_f = 40$)	0.99	2%	125 ms
Conventional ($\eta = 0$, $k_f = 40$)	0.89	50%	unstable system

settling time t_s is smaller in the case of the system with TDFC (Fig. 10(a)-10(d)). Moreover, without TDFC, the settling time increases as the feedback gain increases and the system can even loose stability for relatively higher values of this parameter (Fig. 10(c)). This does not occur for the system under TDFC for which stability is maintained for a wider range of power levels and feedback gains if an appropriate value of the TDFC gain η is used (Fig. 10(d)). Moreover , the steady state THD is the same for both controllers if they are working in their stable periodic regime because the TDFC is a noninvasive controller and the periodic orbit is the same for both systems. Nevertheless, the THD is much smaller in the case of the TDFC controller when the traditional system exhibits subharmonic oscillations and chaotic behavior as it can be observed from the boost inductor current waveforms i_L of Fig. 10(c) and Fig. 10(d). Table II summarizes the performances of both systems in terms of power factor, THD and settling time for the case of $P = 200$ W.

8. Conclusions

The main aim of this study was to characterize the dynamic behavior of a two-stage PFC AC-DC power converter under TDFC. This characterization allowed controlling the line frequency instabilities in this system by appropriately selecting the design parameters within the stability domain. The controller is based on the insertion of a time delay at the feedback voltage path, which can stabilize UPOs lying outside the stability region of the original system.

The use of this method was motivated by the fact that subharmonic and chaotic oscillations contain dominant subharmonic frequencies in the FFT spectrum of the state variables. It was shown that modifying this spectrum by damping certain subharmonic frequencies, makes it is possible to eliminate chaotic and subharmonic motions. The stabilization domain in terms of the design parameters was derived from the averaged nonlinear model and a HB approach. The efficiency of the control technique was demonstrated by numerical simulations using the full order nonlinear model. These simulations are in good agreement with the theoretical predictions. This method only requires the knowledge of the period of the UPO to be stabilized and it can be considered a model independent method. Moreover, the TDFC technique can add advantages to existing commercial control methods in PFC converters by widening the stability range. Namely ACM control is characterized by high gain at the DC component, zero static error for the input current and excellent noise immunity. The result is that average input current tracks the current reference with a high degree of accuracy. This is especially important in high power factor pre-regulators. In PFC applications, the time delay must be

equal to the period of the rectified input voltage to get small THD for the input current.

To summarize, the control of the two-stage AC-DC PFC converter using TDFC in the voltage feedback loop turned out to be a simple but an efficient method for stabilizing the desired periodic orbit. The control of the oscillations in PFC power supplies, in particular, line frequency slow dynamics would be useful because it can easily be experimentally implemented in analog or digital hardware and thus provides a promising control method. However, many practical issues should be considered in a real implementation. First, an exact analog implementation of delayed feedback is not possible because of the need of an infinite memory. However, TDFC has an obvious advantage of a simple experimental implementation if the delay is digitalized. This digital implementation is feasible with enough accuracy in this case because the control technique deals with the line period which is large enough for regular digital processors. This experimental implementation will be the subject of a further study.

Acknowledgements

The authors would like to thank the anonymous reviewers for their valuable comments and suggestions that helped to improve an original version of the paper. This work was partially supported by Agencia EspaÃ±*oladeCooperaciÃ*^{3}*nInternacional*$(AECI)$*undergrantA*/012533/07*andtheSpanishMinister*
$2007 - 67988 - C02 - 02$.

REFERENCES

1. Tse C. K, "Circuit theory of power factor correction in switching converters", *International Journal of Circuit Theory and Applications*, vol. 31, no. 2, pp. 157-198, 2003.
2. GarcÃa O, Cobos J. A, Prieto R., Alou P. and Uceda J., Power Factor Correction: A survey, PESC Record, pp. 8-12, 2001.
3. GarcÃa O, Cobos J. A, Prieto R., Alou P. and Uceda J., Single Phase Power Factor Correction: A Survey, *IEEE Trans. on Power Electronics*, vol. 18, no. 3, pp. 749-755, 2003.
4. Dixon L. H., High power Factor Preregulator for Off-line Power Supplies, Unitrode PSDS Tech. Note, SEM. 600, 1988.
5. Told P. C., UC3854A Controlled Power Factor Correction Circuit Design, Unitrode Application Note, U-134, pp. 3-269-3288, 1997.
6. Huang-Jen Chiu., Hsiu-Ming Huang, Hong-Tzer Yang and Shih-Jen Cheng, An improved single-stage Flyback PFC converter for high-luminance lighting LED lamps, *International Journal of Circuit Theory and Applications*, 36:205-210, 2008.
7. Huang-Jen Chiu, Yu-Kang Lo, Ting-Peng Lee, Ching-Chun Chuang, and Shann-Chyi Mo, A single-stage phase-hifted full-bridge AC/DC converter with variable frequency control, *International Journal of Circuit Theory and Applications*, (2009), Published online in Wiley InterScience (www.interscience.wiley.com). DOI: 10.1002/cta.598
8. A. El Aroudi and M. Orabi, "Control of Oscillations in PFC Power Supplies by Time Delay Feedback", *International Conference on Electric Power and Energy Conversion Systems* (EPECS'09), Sharjah, UAE, November 10-12, 2009.
9. Giaouris D., Banerjee S. Zahawi B. and Pickert V., Control of Fast Scale Bifurcations in Power-Factor Correction Converters, *IEEE Trans. on CAS–II: Express Briefs*, vol. 54, no. 9, 2007.
10. Chu, G. Tse, C.K. Wong S. C., Tan S. C, "A Unified Approach for the Derivation of Robust Control for Boost PFC Converters", *IEEE Trans. on Power Electronics*, vol. 24, no. 11, pp. 2531-2544, 2009.
11. Orabi, M. and Ninomiya T., Non-linear Dynamics of Power Factor Correction Converter, *IEEE Trans. on Industrial Electronics*, no. 6, pp. 1116-1125, 2003.
12. Orabi, O., and Ninomiya, N., Stability investigation of the cascade two-stage PFC converter, *IEICE Transactions on Communications*, vol. E8-B, no. 12, pp. 3506-3514, 2004.

13. Wu X., Tse C. K., Wong S. C. and Lu J., Fast-scale bifurcation in single-stage PFC power supplies operating with DCM boost stage and CCM forward stage, *International Journal of Circuit Theory and Applications*, vol. 34, no. 3, pp. 341-355, 2006.
14. Iu H. H. C., Zhou Y. and Tse C. K., Fast-Scale Instability in a Boost PFC Converter Under Average Current Control, *Int. J. Circ. Theor. Appl.*, vol. 31, pp. 611-624, 2003.
15. El Aroudi A., Orabi M. and MartÃnez-Salamero L., A Representative Discrete-time Model for Uncovering Slow and Fast Scale Instabilities in Boost Power Factor Correction AC-DC Pre-regulators, *Int. J. Bifurcations and Chaos*, vol. 18, no. 10, pp. 3073-3092, 2008.
16. Wong S. C., Tse C. K., Orabi M., and Ninomiya T., The Method of Double Averaging: An Approach for Modeling Power-Factor-Correction Switching Converters, *IEEE Trans. on Circuits and Systems*, vol. 53, no. 2, 2006, pp. 454-462, 2006.
17. Chu G., Tse C.K. and Wong S.-C, Line-Frequency Instability of PFC Power Supplies, *IEEE Trans. on Power Electronics*, vol. 24, no.2, pp. 469-482, 2009.
18. Pyragas K., Control of Chaos via an Unstable Delayed Feedback Controller, *Physical Reviews Letters*, vol. 86, no. 11, pp. 2265-2268, 2001.
19. SchÃ¶ll E. and Schuster H. G., *Handbook of Chaos Control*, Wiley–VCH, 2005.
20. Robert B., Feki M., Iu H. H. C., Control of PWM Inverter Using a Proportional Plus Extended Time-Delayed Feedback Controller, *International Journal of Bifurcation and Chaos*, vol. 16, no. 1, pp. 113-128, 2006.
21. Robert B., Feki M., Iu H. H. C., Adaptive Time-Delayed Feedback for Chaos Control in a PWM Single Phase Inverter, *Journal of Circuits, Systems and Computers,* vol. 13, no. 3, pp. 519-534, 2004.
22. Batlle C., Fossas E., and Olivar G., Stabilization of Periodic Orbits of the Buck Converter by Time-Delayed Feedback, *International Journal of Circuit Theory and Applications*, vol. 27, no. 5, pp. 617–631, 1997.
23. Ott E., Grebogi C., Yorke J. A., Controlling Chaos, *Physical Review Letters*, vol. 64, pp. 1196–1199, 1990.
24. Vasegh N. and Khaki Sedigha A., Chaos control via TDFC in time-delayed systems: The harmonic balance approach, *Physics Letters A*, vol. 373, no. 12, pp. 354-358, 2009.
25. El Aroudi A., Angulo F., Olivar G., Robert B. G. M. and Feki M., Stabilizing a Two-Cell DC-DC Buck Converter by Fixed Point Induced Control, *International Journal of Bifurcation and Chaos*, vol. 19, no. 6, pp. 2043-2057, 2009.
26. Giaouris D., Maity S., Banerjee S., Pickert V., Zahawi B., Application of Filippov method for the analysis of subharmonic instability in dc-dc converters, *International Journal of Circuit Theory and Applications*, no. 10, pp. 899-919, 2009.
27. El Aroudi A. and Orabi M., Stabilizing Technique for AC-DC Boost PFC converter Based on Time Delay Feedback, *IEEE Trans. on CAS–II: Express Briefs*, vol. 57, no. 1, pp. 56-60 2010.
28. Moila J. L and Chen G., Hopf Bifurcation in Time-delayed Nonlinear Feedback Control, in *Proceeding of the 34th conference and decision and control*, New Orleans, 1995.
29. Malakhovski E., Mirkin L., On stability of Second-order Quasi-Polynomials with a Single Delay, *Automatica*, vol. 42, pp. 1041-1047, 2006.
30. Ogata K., Modern Control Engineering , Prentice Hall, 2001.
31. Sebastian J. Lamar D.G. Hernando M.M., Rodriguez-Alonso A. and Fernandez A., "Steady-State Analysis and Modeling of Power Factor Correctors with Appreciable Voltage Ripple in the Output-Voltage Feedback Loop to Achieve Fast Transient Response", *IEEE Trans. on Power Electronics*, vol. 24, no. 11, pp. 2555-2566, 2009.

